Journal of Materials Chemistry A

Accepted Manuscript

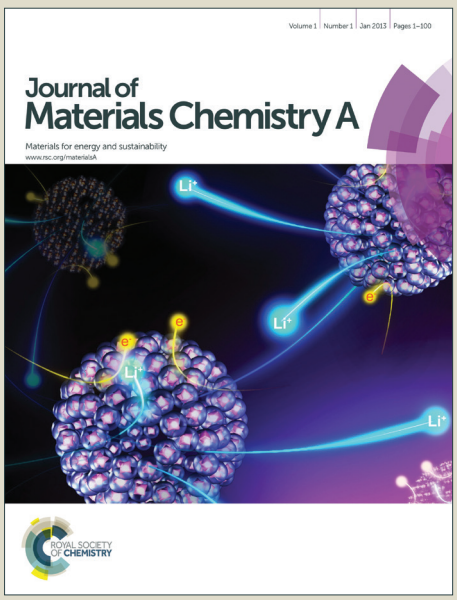

ROYAL SOCIETY OF CHEMISTRY

www.rsc.org/materialsA

Electrochemical behavior and surface structural change of $LiMn_2O_4$ charged to 5.1 V

Daichun Tang‡, Liubin Ben‡, Yang Sun, Bin Chen, Zhenzhong Yang, Lin Gu, and Xuejie Huang*

Charging spinel $LiMn_2O_4$ cathode material to high voltage (> 4.3 V) is a convenient way to obtain more lithium ions for formation of anodic solid-electrolyte-interface in a full cell. In this work, $LiMn_2O_4$ spinel cathode material was charged to 5.1 V for only one cycle during normal cycling (3-4.3 V) to study the impact of high voltage on the electrochemical performance and structure. The electrochemical performance showed that more lithium ions were de-intercalated from the cathode structure during cycling between 3-5.1 V. However, even cycled to high voltage for only one cycle, the surface of the cathode demonstrated a drastic change in atomic-level structure. Via an advanced scanning transmission electron microscopy (STEM), the formation of a layered-like phase was directly observed on the surface of spinel $LiMn_2O_4$ charged to high voltage, implying instability of the spinel structure at high charge voltage. This observation contradicts to the conventional wisdom that the spinel structure is more stable than the layered structure during lithium intercalation. X-ray photoelectron spectroscopy (XPS) results showed a small amount of manganese with lower oxidation states after being charged to 5.1 V, suggesting an accelerated speed of manganese dissolution.

1. Introduction

Lithium ion batteries have been widely used for applications in various portable electronic devices, such as laptop computers, mobile phones, and they are now targeting the market of hybrid electronic vehicles (HEVs) and electronic vehicles (EVs).[1, 2] One of the most promising candidates for lithium ion batteries is spinel $LiMn_2O_4$ cathode material due to its several advantages such as low cost, environmentally benignity, high cell potential and high rate capability.[3] Unfortunately only ~80% of lithium ions can be de-intercalated from this cathode material at a voltage range of 3-4.3 V, giving a practical capacity of only ~120 mAh/g,[4, 5] Nearly ~20% lithium ions remain in the lattice and do not take part in the intercalation during cycling, resulting in not only a lowered efficiency of lithium utilization but also a potential safety problem. It is known that if a lithium ion battery is overcharged in case of abuse, the remaining lithium ions in the cathode material may be

deintercalated from the structure and deposit on the anode surface, causing internal short circuit of the battery.[6, 7]

The lithium ions that remain in the $LiMn_2O_4$ cathode material can be further de-intercalated if cycling voltage is increased (> 4.3V). However, several phenomena may occur during charging to high voltage. Oxidation of electrolyte has been suggested at high cycling voltages,[8, 9] forming an ion-blocking surface film on the cathode and increasing the impedance of lithium diffusion. This side reaction may deteriorate the cycling performance of $LiMn_2O_4$. It is also known that with increasing the cut-off charge voltage, the speed of dissolution of Mn increases which results in a loss of electrode material and consequently a decrease in the cycling performance.[10-12] The crystal structure, particularly the surface structure may be affected by the high charge voltage. However, the surface structural change of $LiMn_2O_4$ cycling to higher voltage has not been adequately addressed.

Charging the cathode material to high voltage may induce instability of the crystal structure which is usually initiated from the local surface area.[13-17] Many previous structure studies using characterization techniques such as powder diffractions only obtained the information of overall structure but lacked the details of local structure. The overall structure of $LiMn_2O_4$ was reported to remain as spinel but vary only slightly in lattice parameters during electrochemical cycling, based on XRD and ND studies.[18-21] Recently, the spherical aberration (Cs) corrected scanning transmission electron microscopy (STEM) with atomic resolution has been proved to be a powerful technique to determine the local atomic-level information of battery materials.[22-26] It can directly provide not only the bulk but also surface structure information of battery materials during electrochemical cycling.

For a full Li-ion cell, the anode used is usually graphite which always needs ~10% of lithium ions for formation of anodic solid-electrolyte-interface (SEI).[27, 28] It is strongly desired to know if some of the remaining lithium ions in the $LiMn_2O_4$ cathode material can be de-intercalated from the cathode to compensate for the lithium ions for SEI. This will increase the utilization of lithium ions as well as safety of the Li-ion cell. Thus in this study, the spinel $LiMn_2O_4$ cathode material is charged to 5.1 V for only one cycle before normal 3-4.3 V cycling for de-intercalating more lithium from the cathode. The lithium which could not be intercalated back to the cathode structure during

the discharge process can be used for formation of anodic solid-electrolyte-interface (SEI). The influence of charging to 5.1 V on the electrochemical performance and the surface structural change is discussed.

2. Experimental

2.1 Materials Preparation

$LiMn_2O_4$ was prepared using the solid state method. The mixture of stoichiometric amounts of Li_2CO_3 (Alfa Aeasar) and EMD (Xiangtan Electrochemical Scientific Ltd.) was used as the starting material. The mixture was heated for 10 h at 900 ^oC in an oxygen atmosphere followed by slow cooling to room temperature.

2.2 Materials characterization

The transmission electron microscopy (TEM) and the selected area electron diffraction (SAED) were conducted on FEI Tecnai F20. The chemical composition of $LiMn_2O_4$ samples in the discharged states before and after charged to high voltage was determined by an inductively coupled plasma/atomic emission spectrometer (ICP/AES). Microstructures were studied by a scanning electron microscopy (SEM, JEOL JSM-7600F, 15kV). The X-ray photoelectron spectroscopy (XPS) spectra were recorded with a spectrometer having Mg Kα radiation (ESCALAB 250, Sigma Probe, Thermo VG Scientific Co. Ltd.). All binding energies reported were corrected using the signal for the carbon at 284.8 eV as an internal standard. The peak-fitting and quantitative evaluation was performed with the CasaXPS software. The background was corrected using the Shirley method. The change in manganese valence state at different charged and discharged states were interpreted from the XPS data. The electrochemical impedance spectroscopy (EIS) of the cell, which was discharged to 3V, was measured using a Novocontrol impedance analyzer (Nata-N). The amplitude of the AC signal was 5 mV over frequency range between 100 kHz and 0.1 Hz. An aberration-corrected scanning transmission electron microscope JEM ARM200F (JEOL, Tokyo, Japan) equipped with two CEOS (CEOS, Heidelberg, Germany) probe aberration correctors was used to probe the structure at atomic scale. Z-contrast annular bright field (ABF) and high-angle annular dark field (HAADF) imaging was performed in thin specimen regions with a probe convergence angle of 25 mrad. The collection angle of them is 12-24 mrad and

70-250 mrad, respectively. For each sample, several particles are analysized and the representative images are selected for analysis.

2.3 Electrochemical Tests

Electrodes was prepared by mixing $LiMn_2O_4$ with conductive acetylene black and polyvinylidene fluoride (PVdF) binder in a weight ratio of 8:1:1. The electrolyte used was EC (ethylene carbonate) and DEC (diethyl carbonate) (1:1 by volume)/1M $LiPF_6$. Lithium metal disc was used for the anode. Cells were assembled in an argon-filled glove box. Charge and discharge tests of the cells were carried out at room temperature. Two charge and discharge strategies were performed on the batteries: strategy one, charge and discharge within the operating voltage range of 4.3-3 V with a current density of 0.2 C; strategy two, charge and discharge within operating voltage range of 4.3-3 V with a current density of 0.2 C except for the 7^{th} cycle whose voltage range was 3-5.1 V with the same current density. For evaluating the cathode materials, the cells were disassembled in an argon-filled glove box, and the cathode was rinsed with DMC solution for removing the electrolyte salt.

3. Results

3.1 Structure and morphology

The $LiMn_2O_4$ in the experiment has been proved to be a pure cubic phase by Rietveld refinement of powder X-ray diffraction patterns. The crystal structure of the pristine $LiMn_2O_4$ powder was investigated initially as a reference. Fig.1a presents a typical SEM image of the $LiMn_2O_4$ particles. It can be seen that the pristine $LiMn_2O_4$ was composed of well-defined octahedral crystals. Typical images of High Resolution Transmission Electron Microscopy (HRTEM) and Selected Area Electron Diffraction (SAED) patterns are shown in Fig.1b-d. Fig.1b presents a HRTEM image of the surface region of the pristine $LiMn_2O_4$ particle, and the inset shows a Bright Field (BF) image of the whole particles. The d-spacing in the bulk region is ~0.47 nm, which is close to the d-spacing of the (111) plane of the spinel $LiMn_2O_4$ structure. A SAED (Fig.1c) pattern obtained from the bulk region can be indexed as diffraction from a [112] zone-axis of the spinel structure. A fast Fourier transformation (FFT) from orange box as indicated in Fig.1b results in a pattern that is identical to the SAED obtained from the bulk. Therefore, it can be concluded that the crystal structure of the

pristine sample is homogeneous from the bulk to the surface.

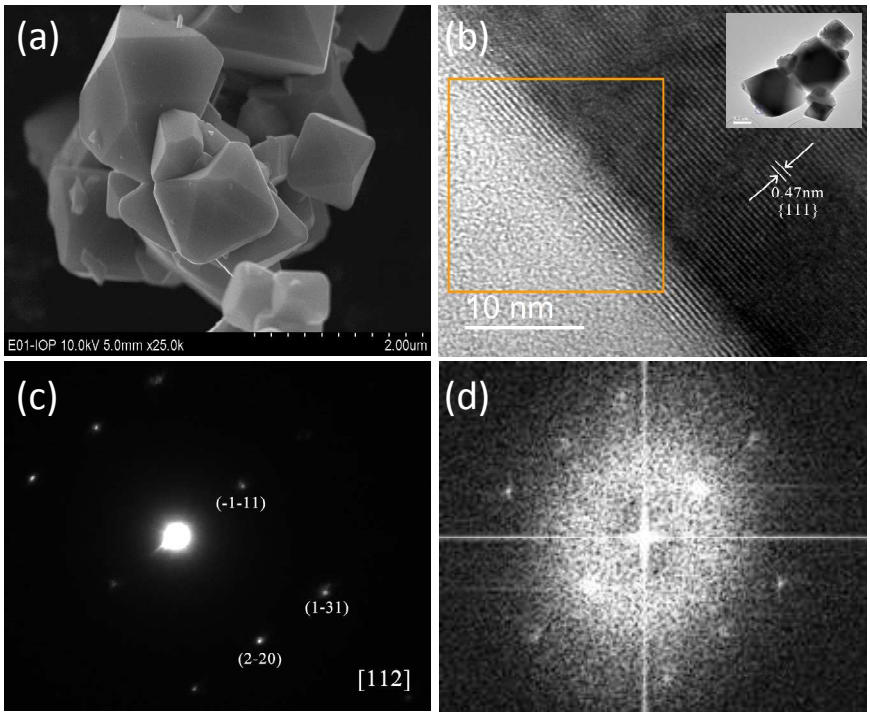

Fig.1 (a) A typical SEM image of pristine $LiMn_2O_4$; (b) HRTEM image of the surface region of a pristine $LiMn_2O_4$ particle. The inserted image shows the overview of the several particles; (c) Diffraction patterns of the bulk region of the particle; (d) Fast Fourier transform from the orange box region as indicated in b.

3.2 Ex-situ XRD Data Analysis

The voltage profile of the $LiMn_2O_4$ cathode material charged to 5.1 V and the variations of lattice parameters at different states are shown in Fig.2a and 2b, respectively. A single-phase process was confirmed during the charge, as suggested from XRD results. It has been reported that whether the process is single-phase or two-phases, depending on the sample history.[4] The lattice parameter decreased gradually during charge, especially at the voltage below 4.3 V, indicating that most of the lithium was extracted at the voltage below 4.3 V. The capacity of the $LiMn_2O_4$ cathode material in the voltage range of 3-4.3 V was ~110 mAh/g, suggesting that ~0.25 mol Li remained in the lattice. This is based on the theoretical capacity of ~ 148 mAh/g and attribution of capacity to lithium ions. Further increase the voltage from 4.3 V to 5.1 V, the lattice parameter decreased slightly, suggesting that extra Li was extracted from the structure. This slow decrease of lattice parameters due to further de-intercalation of lithium ions at high voltage is in agreement with previous reports. [19, 20]

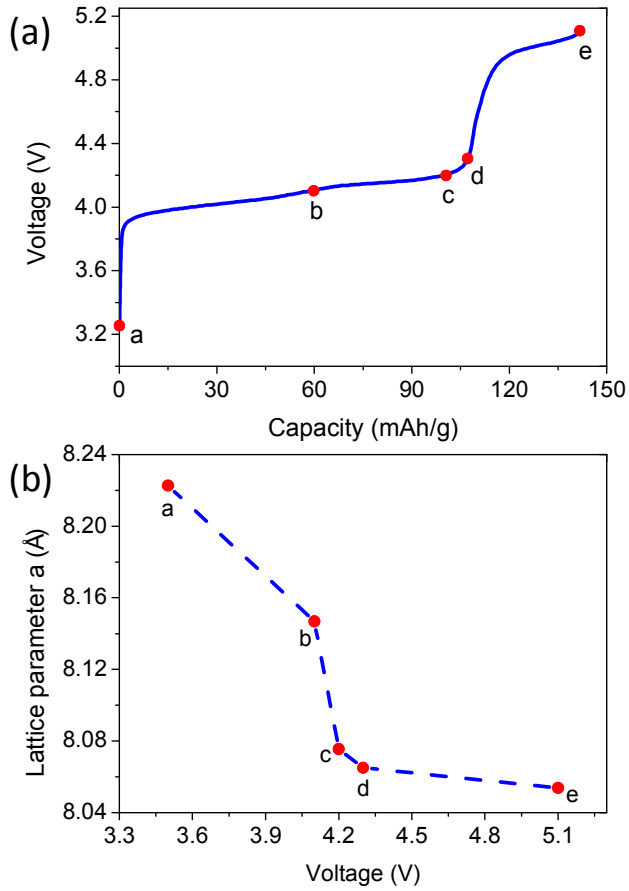

Fig.2 (a) Charge profile of $LiMn_2O_4$ cathode material charged to 5.1V; (b) Variation of lattice parameter a vs. voltage.

3.3 Electrochemical Characterization, Chemical Analysis

In order to investigate the effect of high charge voltage on the electrochemical performance and structure of $LiMn_2O_4$ cathode, the cell was charged to 5.1 V on the 7th cycle. After the 7th cycle, the upper cut-off voltage was kept at 4.3V in the following cycles (strategy 2). The normal charge-discharge (3-4.3 V, strategy 1) profile is also displayed in Fig.3 for comparison. Before being charged to 5.1 V (1-6th cycle), $LiMn_2O_4$ delivered a stable and reversible discharge capacity of ~109 mAh/g. It increased to ~ 123.6 mAh/g after being charged to 5.1 V (7th cycle), which indicates that an extra amount of lithium can be extracted and reinserted back into the structure after being charged to 5.1 V. However, the following cycle (8th cycle) showed slightly polarization of the electrode (Fig.3a). Differential capacity plots of the three cycles (6th, 7th, 8th of strategy 2) exhibited two oxidation peaks located at about 4.04 V, 4.17 V, and two reduction peaks located at about 4.00 V, 4.11 V between the voltage of 3.5 V and 4.5 V. These reduction and oxidation peaks are similar to that reported previously.[10] After being charged to 5.1 V, an extra broad peak located at about 5.03

V can be observed, which may be due to the oxidation of O^{2-} and de-intercalation of lithium ions.[29] as well as side reaction such as oxidation of electrolyte.[30, 31]. It should be noted that, the cycling profile of the $LiMn_2O_4$ cathode material after being charged to 5.1 V deteriorated rapidly (Fig.S1). It only showed capacity retention of ~77.3% after 50th cycle, while it is ~93.4% for the normal charge-discharged sample.

According to the ICP-AES analysis, the ratio of Li:Mn at discharged state before and after being charged to 5.1 V (6th, 7th for strategy 2) were 1.00 : 2.00 and 0.94 : 2.00 respectively. This suggests that, although extra lithium ions could be extracted after being charged to 5.1 V, 0.06 mol lithium ions (~9 mAh/g) may not be inserted back into the cathode during discharge. This demonstrates that charging to high voltage, even for one cycle, has a significant impact on the battery performance and variation of lithium content in the cathode structure.

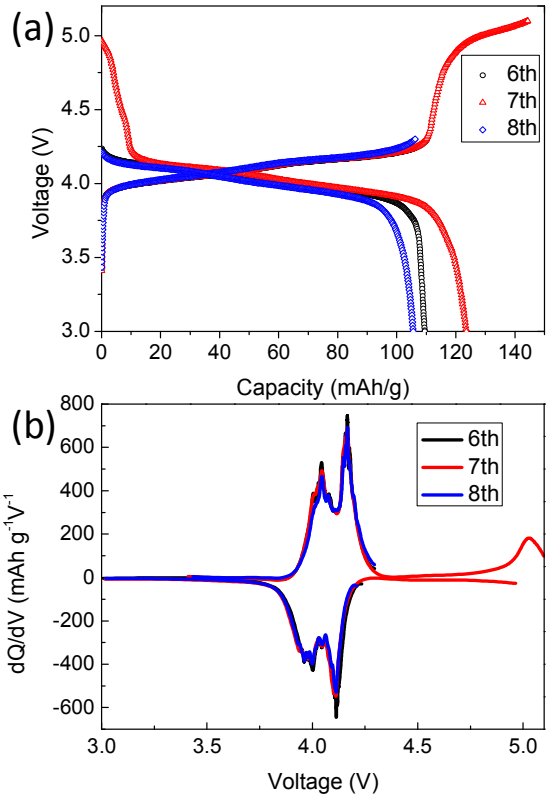

Fig.3 (a) Charge and discharge profiles for the 6th, 7th, 8th cycles of strategy 2; (b) Differential capacity (dQ/dV) plots for the 6th, 7th, 8th cycles of strategy 2;

3.4 X-ray photoelectron spectroscopy (XPS) and Electrochemical Impedance measurement (EIS) Analysis

X-ray photoelectron spectroscopy (XPS) can provide a semi-quantitative analysis on the valence

state of specific ions in specific areas.[32] Fig.4a shows the XPS spectra for Mn 2p at different states of (dis)charge. All the spectra were normalized to $Mn2p_{3/2}$ for better comparison. Two main peaks, which correspond to Mn $2p_{3/2}$ and $2p_{1/2}$ respectively, were observed in the spectra for the pristine $LiMn_2O_4$.[33] After being charged to 5.1 V, the Mn $2p_{3/2}$ showed asymmetric characteristics, which can be interpreted as multiplet splitting from Mn^{4+} state.[33] The discharged $LiMn_2O_4$ exhibited similar spectral features with the pristine $LiMn_2O_4$. In order to obtain detailed information on the valence states of Mn at different states, curve fitting was conducted on the Mn $2p_{3/2}$ spectra (Fig.4b-d), and the details of the fitting are shown in Supporting Information (Section S1). The fitting parameters are in agreement with that of Biesinger's (Table S1-S4 in Supporting Information).[33] The results indicate ~48.7% Mn^{4+}, ~48.9% Mn^{3+} and ~2.4% Mn^{2+} were present in the pristine $LiMn_2O_4$ (Fig.4b), which is in agreement with the valence distribution of Mn in typical $LiMn_2O_4$. After being charged to 5.1 V (Fig.4c), Mn^{4+} was dominant in $Li_xMn_2O_4$ (~ 63.2%). However, there was still ~ 27.4% Mn^{3+} and ~9.3% Mn^{2+} presented in the charged sample. This is contracted to the conventional wisdom that the amount of Mn^{3+} and Mn^{2+} should be negligible in $Li_xMn_2O_4$ at the charged state. After being discharged to 3.0 V (Fig.4d), the valence distribution of Mn was similar to the pristine $LiMn_2O_4$.

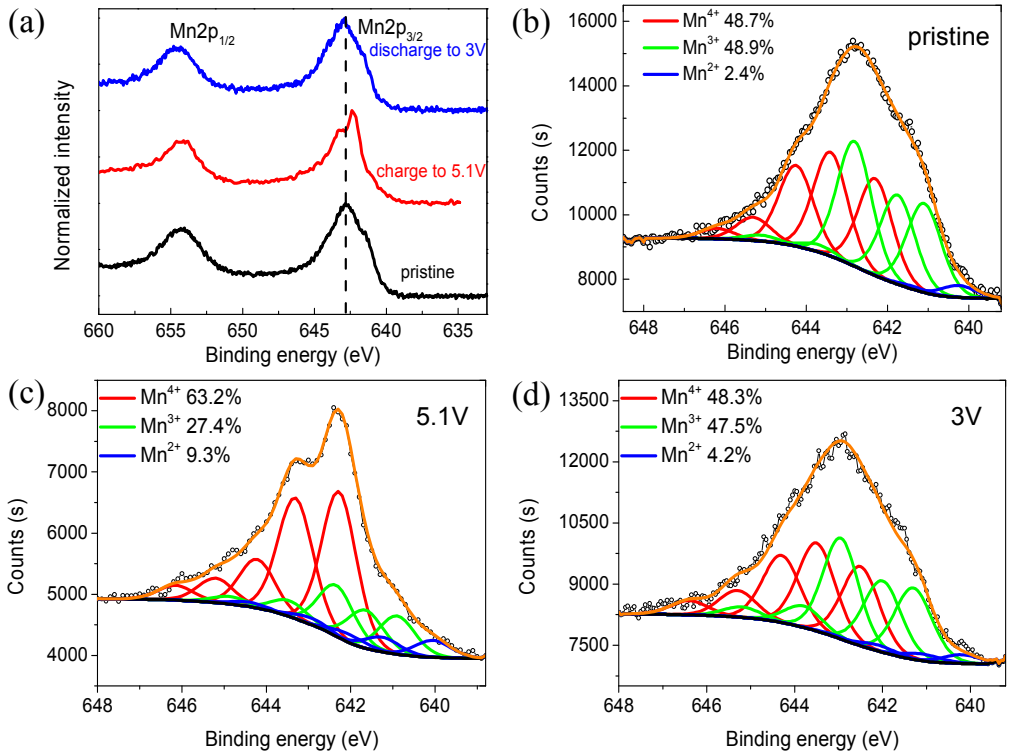

Fig.4 (a) Mn 2p spectra for $LiMn_2O_4$ at different states (pristine, charged to 5.1 V, discharged to 3 V); fitting spectra of

(b) pristine $LiMn_2O_4$; (c) $LiMn_2O_4$ charged to 5.1 V; (d) $LiMn_2O_4$ discharged to 3 V after being charged to 5.1 V.

The reaction kinetics of $LiMn_2O_4$ before and after being charged to 5.1 V was investigated by electrochemical impedance measurements (EIS), and the results are shown in Fig.5. The impedance spectra of a typical cell consisted of one depressed semicircle in the high frequency region and a spike in the low frequency region. The intercept at the Z′ axis corresponds to the ohmic resistance (Rs) i.e. electrolyte resistance. Usually two semicircles are observed for cathode materials during electrochemical cycling with the medium frequency one attributed to the charge transfer impedance (Rct) and the high frequency one attributed to the surface film impedance (Rf).[34, 35] It should be noted that, often, only one semicircle is observed, even in cathode materials charged to high voltage.[36] This may be possibly due to the similar time constant of the charge transfer and surface film.[37] The spike in the low frequency region represents the Warburg impedance (Zw), which is associated with lithium-ion diffusion in the particles. Note that the frequency range applied for the impedance measurements in this study is 100 mHz-100 KHz, it is unlikely that any additional semicircles present in the lower frequency region, based on the frequency range used and the shape of the spike observed.[37] Nevertheless, the Rs value did not show significant change after being charged to high voltage, but Rct+Rf for the discharged state of 7th cycle is ~190 Ω, more than three times than that of the discharged state of 6th cycle.

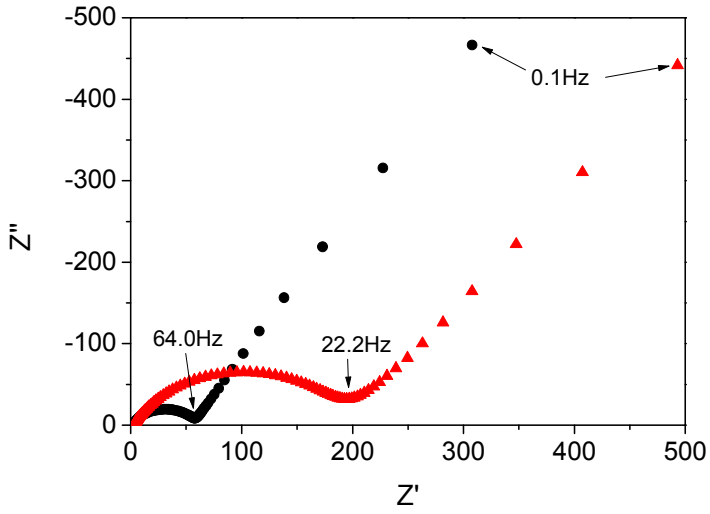

Fig.5 EIS spectra for $LiMn_2O_4$ in the discharged states before and after charge to 5.1 V. The equivalent circuit and the values for Rs and Rct are shown in the figure.

3.5 Surface Structural Change

Employing the aberration-corrected scanning transmission electron microscopy (STEM) technique equipped with annular bright field (ABF) and high-angle annular dark field (HAADF) detectors, the crystal structure after (dis)charge can be identified directly at atomic scale.[38] Fig.6 shows the crystal structure of spinel $LiMn_2O_4$ viewed along the [110] direction, which clearly exhibits the separated columns of Li, Mn and O atoms. As indicated by the arrows, two different Mn columns are assigned to Mn1 and Mn2, since the stacking density of Mn1 column is twice that of Mn2 column.

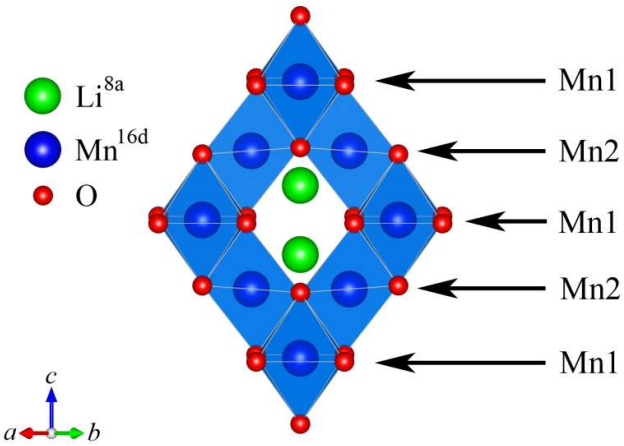

Fig.6 Demonstration of diamond structure of $LiMn_2O_4$ viewed along the [110] crystallographic direction. Blue spheres represent Mn, red for O, green for Li and MnO_6 octahedrons are blue. Li occupies 8a and Mn occupies the 16d site. Two different Mn columns are assigned: Mn1, Mn2, as they have different stacking density.

We have recently shown that spinel $LiMn_2O_4$ cathode undergoes a surface structure evolution during cycling between 3.0-4.3 V. The crystal structure of pristine $LiMn_2O_4$ is homogeneous from the bulk to the surface, but Mn_3O_4 phase formed at the surface of $LiMn_2O_4$ during the charge process. The amount of Mn_3O_4 reaches maximum at the end of charge, while decreases to be negligible during the subsequent discharge.[39] Here we further extend the structure study of $LiMn_2O_4$ cathode charged to 5.1 V and discharged to 3 V. After being charged to 5.1 V, the local atomic-level structure is very different to the spinel structure, particularly at the surface region. The most striking difference between the surface region and the bulk is the appearance of a layered-like structure in the surface region (Fig.7a, 7d). The distance between the two layers indicated by the green arrows is 4.7 Å. This layered-like structure can be clearly observed in the magnified image (Fig.7b, 7e). All spots along the white line in Fig.7b, in particular, show nearly the same contrast, which is different from the bright and dark points alternatively arranged in the bulk. This structure is likely corresponding to [110] direction of the O3-layered structure (Fig.7c, 7f). The layered-like structure

is not homogeneously distributed at the particle surface since its thickness varies from particle to particle with a rough range between 1 nm-5 nm, (Fig.S2 in supporting information). This may suggest the phase transformation from spinel to layered-like is kinetically controlled. In addition, only a small amount of remaining Mn_3O_4 structure can also be detected in the sub-surface, as indicated by the white arrow in Fig. 7. This is different to the cathode charged to 4.3 V which showed a significant amount of defective spinel Mn_3O_4 phase on the surface.

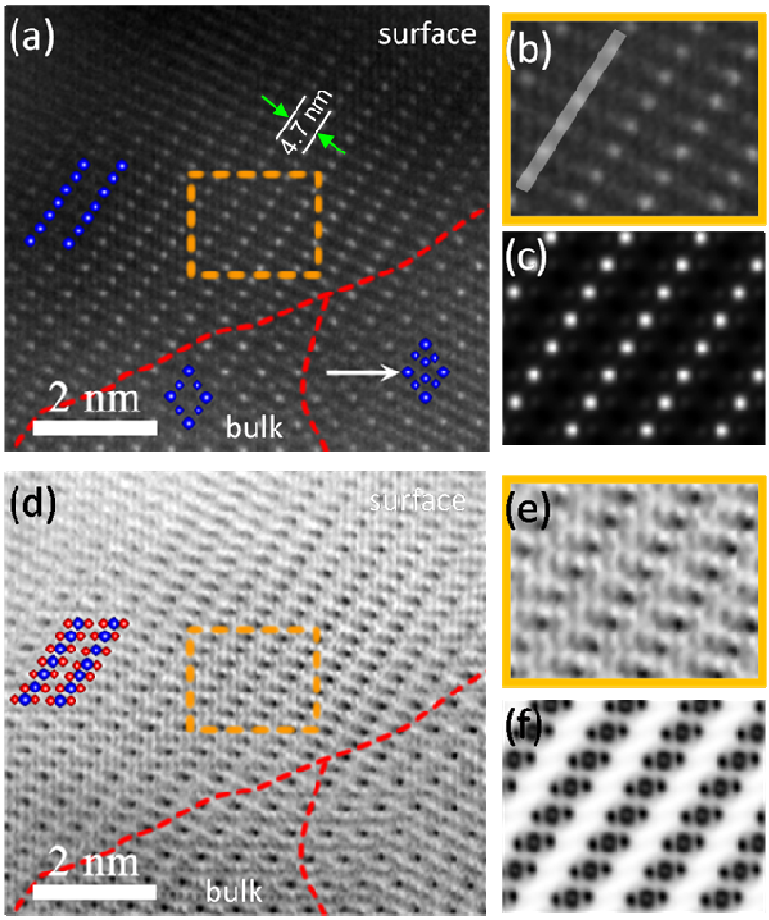

Fig.7 HAADF and ABF images taken along the [110] zone axes of the $LiMn_2O_4$ electrode charged to 5.1 V. HAADF image (a) and ABF image (d) of $LiMn_2O_4$ electrode charged to 5.1V. The white arrow indicates the Mn_3O_4 structure, the red and green spheres represent O and Mn respectively; Figure b and e show the magnified regions as indicated as orange dashed squares in a and d, respectively. The white line indicated the same contrast of all dots; simulated ADF image (c) and ABF image (f) corresponding to Figure b and e, respectively

The layered-like structure was not observed from the surface area of the $LiMn_2O_4$ when the cathode was discharged to 3 V from 5.1 V (Fig.8). The surface structure was almost identical to the bulk, showing a typical spinel structure. Note that the surface region showed slight contrast at 8a

site.

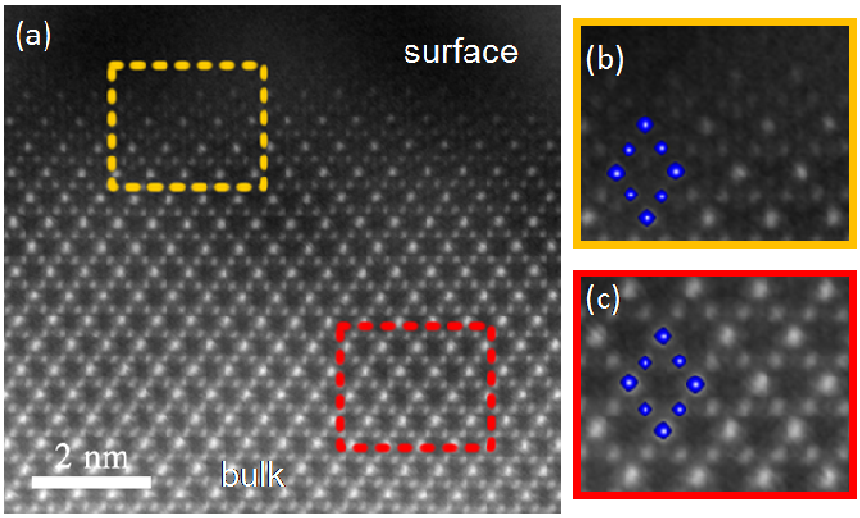

Fig.8 HAADF image taken along the [110] zone axes of the $LiMn_2O_4$ electrode discharged to 3.0 V after being charged to 5.1V. Figure b and c show the magnified regions as indicated as yellow-dashed square and red-dashed square, respectively, in Figure a.

4. Discussion

According to above experimental results, more lithium could be extracted from the structure after charging $LiMn_2O_4$ cathode material to 5.1 V (Strategy 2, Fig.3). However, there was 0.06 mol lithium per formula unit could not be re-intercalated back to the cathode during the following discharge, indicating an irreversible intercalation process. Although the lost 0.06 mol lithium can be used to form the anodic SEI in full cell,[27, 28] the cycling performance in the following normal charge/discharge (3-4.3V) degraded faster than that of normal cycled sample (Strategy 1, Fig.3). The origin of the capacity degradation mechanism in overcharged $LiMn_2O_4$ may be related to cell polarization After being charged to high voltage, the electrolyte decomposition accelerated, inducing the formation of surface phases between electrode and electrolyte, which will cause cell polarization. It had been widely acknowledged that capacity degradation in many cases is due to the formation of surface phases between electrode and electrolyte, accompanied by lowered mobilities of lithium ions when diffuse through the surface phases.[10, 35]

After being charged to 5.1 V, the content of Mn^{2+} increased, which is explained by two possibilities. The first one is attributed to the destabilization of lattice during charge by evolution of a small amount of O_2 and formation Mn_3O_4 phase, which is consistent with our previously results.[39]

The Mn_3O_4 phase is clearly detected after being charged to high voltage (Fig.7), which has 1/3 of Mn^{2+} ions, thus its existence at the surface contributes to the Mn^{2+} signal of XPS (Fig.4). However, compared to $LiMn_2O_4$ charged to 4.3 V in our recent work,[39] the Mn^{2+} signal of $LiMn_2O_4$ charged to 5.1 V is larger, while the amount of Mn_3O_4 are even lower, thus we suspect that other forms of Mn^{2+} may be exist at the surface area after being charged to high voltage. In the surface area, Mn^{2+} may exist as Mn-F species (presumably MnF_2).[40] After being charged to high voltages, Mn dissolution and decomposition of $LiPF_6$ accelerated, which may cause formation of MnF_2 at the surface and contribute to the Mn^{2+} signal of XPS. The decrease of Mn^{2+} during the discharge process may be caused by the dissolving of Mn^{2+}.

The structural change associated with overcharge was identified by atomic-resolved STEM imaging, which illustrated a layered-like structure on the surface of $LiMn_2O_4$ particle after being charged to 5.1V (Fig.9). This layered-like phase only appeared on the outmost surface of $LiMn_2O_4$ particles thus it could not be conveniently detected by many characterization techniques, e.g. X-ray diffraction. In fact, the spinel to the layered-like structure transformation has not been widely observed. In contrast, the layered structure is believed to be unstable and it gradually transforms to the spinel structure during delithiation.[16, 17] The extend of transformation from the layered to the spinel during cycling is so significantly in some samples, e.g. $LiMnO_2$, xLi_2MnO_3•$(1-x)LiMnO_2$, that it can be easily determined via powder X-ray diffraction.[41-43] To the best of our knowledge, the spinel to the layered structure transformation has only been observed in electrode materials for sodium ion battery, Tarascon *et al*[44] and Yabuuchi *et al*[45] reported that sodium ions could be inserted into the chemically charged spinel phase (λ-MnO_2), leading to partial phase transition from the spinel to the monoclinic layered O′3-type Na_yMnO_2 phase. Yang *et al*. reported that structure transformation from the spinel Mn_3O_4 to the layered structure birnessite ($Na_\delta MnO_x$•nH_2O) took place in neutral electrolyte Na_2SO_4 by electrochemical cycling.[46] Our observations based on STEM, however, suggest for the first time that transformation from the spinel to the layered-like structure may take place in $LiMn_2O_4$ cathode materials for lithium ion batteries.

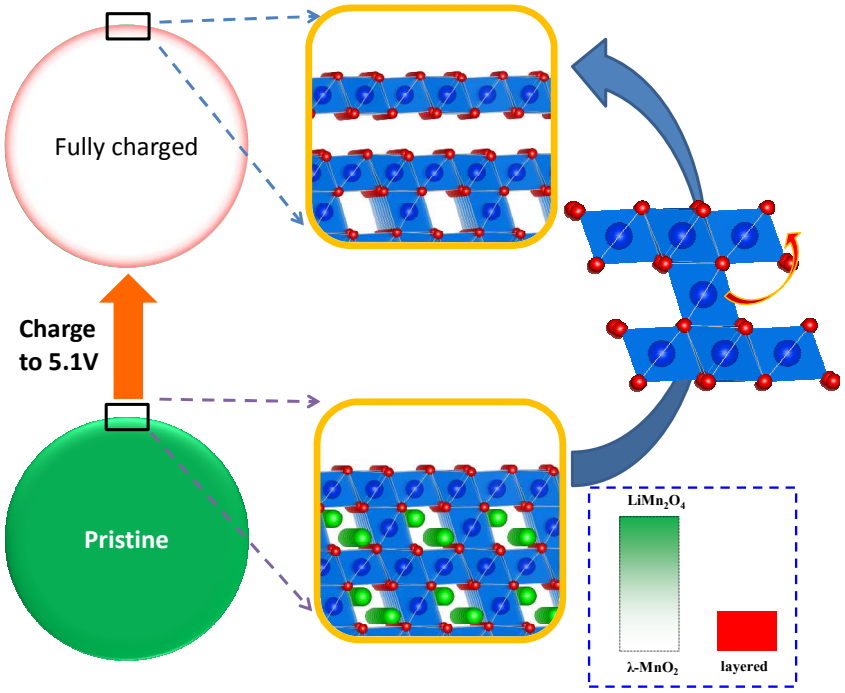

Fig.9 Schematics of phase transition from spinel to layered-like structure on the surface of $LiMn_2O_4$ after being charged to 5.1 V. The lithium concentration of $Li_xMn_2O_4$ is represented by the transparency of green colour where fully transparent green colour indicates λ-MnO_2 and fully opaque green colour indicates $LiMn_2O_4$. The layered-like phase is indicated by the red colour. During the charge process, the layered-like phase forms at the surface region after being charged to 5.1V. Transformation from spinel to layered structure requires the cation migration from one octahedral site to another, as indicated by the red arrow.

The appearance of the layered-like structure may be a consequence of instability of highly charged $LiMn_2O_4$. Theoretical studies have suggested that MnO_2 with layered structure is energetically favorable compared to the fully delithiated $LiMn_2O_4$ (λ-MnO_2).[47] However, transformation from the spinel to the layered structure requires the cation migration from one octahedral site to another, through an intermediate tetrahedral site.[48] This process has a high energy barrier and thus less possible, unless it is aided by the charge disproportionation in the tetrahedral site. In the fully delithiated $LiMn_2O_4$, most of the Mn are +4 and therefore, the Mn passage through the tetrahedral is energetically unfavorable. This explains why the metastable (λ-MnO_2) retains the original structure in bulk phase. On the particle surface, however, the valence of Mn is lowered indicated by XPS. The significant amount of Mn^{3+}, which enables the charge disproportionation process, makes the manganese rearrangement possible. The low Mn valence on the particle surface indicates the oxygen deficient, which originates from the structural instability at over-delithiated state. The layered-like structure is closely related to the layered $Li_xMn_yO_2$, based on the distance of

two layers and the FFT image corresponding to the surface structure.[49, 50] The formation of layered-like phase may be a consequence of further lithium delithiation from the lattice and associated severe destabilization of surface structure during charging to high voltages. It is also possible that the appearance of the layered-like structure may be the result of electrolyte oxidation and Li^+-H^+ exchange, which alters arrangement of oxygen and manganese in the surface. It was reported that Li^+-H^+ exchange occurs in Li_2MnO_3, changing the stack sequence of oxygen from O3 to the P3 stacking.[51-53] In our study, after being charged to high voltage, the remaining Li^+ in the spinel structure may also exchange with H^+, rearranging the surface atoms. Since the thickness of layered-like phase is only less than 5 nm, which is unlikely to be related to the broad peak at around 5 V in the differential curve (Fig.3b).

The mechanism of disappearance of layered-like structure during the following discharge process is unknown and needs further investigations (Fig. 8). Two possible reaction paths could be proposed. One possibility is that the whole layered-like structure at the surface decomposed in the discharge process. The other is transformation from the layered to the spinel during lithium ions intercalation in the discharge process. Since the spinel structure is more stable after lithium intercalation, the layered to the spinel transformation always takes place in the traditional layered and lithium-rich materials.[13-17] Nevertheless, the results here demonstrate that the surface structure of $LiMn_2O_4$ is complicated and different from that of the bulk, particularly when $LiMn_2O_4$ is charged to high voltage. The difference may not be easily probed by other techniques due to the size is only to several atomic layers, but it can be effectively distinguished by STEM.

The appearance/disappearance of layered-like structure during charge/discharge process may contribute to the deterioration of electrochemical performance, and indicate the instability of spinel structure after charge to high voltage. The structure stability of $LiMn_2O_4$ spinel structure is of vital importance for reversible intercalation of lithium ions. On charge to high voltage, $LiMn_2O_4$ is particularly vulnerable to structure degradation. Our studies of $LiMn_2O_4$ charged to 5.1 V not only demonstrate a rich surface chemistry of this well-studied cathode material but also suggest that stabilization of the surface structure by doping or coating is the key to improve its electrochemical performance if more lithium ions are utilized.

5. Conclusions

In summary, we have combined XPS, EIS, TEM, SAED, STEM to investigate the influence of charge to 5.1 V on the electrochemical performance and structural evolution of the spinel $LiMn_2O_4$ cathode material. Charging $LiMn_2O_4$ to 5.1 V de-intercalate more lithium ions from the spinel structure and de-intercalated 0.06 mol lithium ions could not get back into the structure on the subsequent discharge cycle. These 0.06 mol lithium ions can be used to compensate for that consumed to form anodic SEI in a full cell using graphite as anode. Oxidation state of the surface Mn after charge to 5.1 V shows a small amount of Mn^{3+} and Mn^{2+}, speeding up manganese dissolution. The appearance/disappearance of layered-like structure during charge/discharge process indicates the instability of $LiMn_2O_4$ structure, especially the surface. Our work shed light on the importance of understanding the surface structural evolution of cathode material. It further suggests that modification and stabilization of the surface crystal structure, especially at charged state, are vital to develop satisfied high voltage cathode material for Li-ion batteries.

Acknowledgments

This work was supported by the National Basic Research Program of China (Grant No. 2013CB934002) and the "Strategic Priority Research Program" of the Chinese Academy of Sciences (Grant No. XDA01020304).

Notes and references

Beijing National Laboratory for Condensed Matter Physics, Institute of Physics, Chinese Academy of Science, Beijing 100190 China

* To whom correspondence should be addressed: E-mail: xjhuang@iphy.ac.cn (X. Huang).

‡ These authors contributed equally to this work

†Electronic Supplementary Information (ESI) available: Notes on XPS fitting and the parameters used for fitting, etc.

1. Tarascon, J. M.; Armand, M. *Nature* **2001,** 414, (6861), 359-367.
2. Xiong, L.; Xu, Y.; Tao, T.; Song, J.; Goodenough, J. B. *J Mater Chem* **2012,** 22, (47), 24563-24568.
3. Dai, Y. L.; Cai, L.; White, R. E. *Journal of the Electrochemical Society* **2013,** 160, (1), A182-A190.
4. Xia, Y. Y.; Yoshio, M. *Journal of the Electrochemical Society* **1996,** 143, (3), 825-833.
5. Tarascon, J. M.; Guyomard, D. *Electrochimica Acta* **1993,** 38, (9), 1221-1231.
6. Lu, W.; López, C. M.; Liu, N.; Vaughey, J. T.; Jansen, A.; Dennis W., D. *J Electrochem Soc* **2012,** 159, (5), A566-A570.
7. Perkins, R. D.; Randall, A. V.; Zhang, X.; Plett, G. L. *Journal of Power Sources* **2012,** 209, (0), 318-325.
8. Patoux, S.; Daniel, L.; Bourbon, C.; Lignier, H.; Pagano, C.; Le Cras, F.; Jouanneau, S.; Martinet, S. *Journal of Power*

Sources **2009,** 189, (1), 344-352.

9. Zhong, Q.; Bonakdarpour, A.; Zhang, M.; Gao, Y.; Dahn, J. R. *J Electrochem Soc* **1997,** 144, (1), 205-213.
10. Xia, Y. Y.; Zhou, Y. H.; Yoshio, M. *Journal of the Electrochemical Society* **1997,** 144, (8), 2593-2600.
11. Jang, D. H.; Shin, Y. J.; Oh, S. M. *J Electrochem Soc* **1996,** 143, (7), 2204-2211.
12. Wang, L.-F.; Ou, C.-C.; Striebel, K. A.; Chen, J.-S. *J Electrochem Soc* **2003,** 150, (7), A905-A911.
13. Xu, B.; Fell, C. R.; Chi, M. F.; Meng, Y. S. *Energy & Environmental Science* **2011,** 4, (6), 2223-2233.
14. Boulineau, A.; Simonin, L.; Colin, J. F.; Canevet, E.; Daniel, L.; Patoux, S. *Chemistry of Materials* **2012,** 24, (18), 3558-3566.
15. Boulineau, A.; Simonin, L.; Colin, J. F.; Bourbon, C.; Patoux, S. *Nano Letters* **2013,** 13, (8), 3857-3863.
16. Jung, S.-K.; Gwon, H.; Hong, J.; Park, K.-Y.; Seo, D.-H.; Kim, H.; Hyun, J.; Yang, W.; Kang, K. *Advanced Energy Materials* **2014,** 4, (1), n/a-n/a.
17. Hwang, S.; Chang, W.; Kim, S. M.; Su, D.; Kim, D. H.; Lee, J. Y.; Chung, K. Y.; Stach, E. A. *Chemistry of Materials* **2014,** 26, (2), 1084-1092.
18. Richard, M. N.; Koetschau, I.; Dahn, J. R. *J Electrochem Soc* **1997,** 144, (2), 554-557.
19. Sun, X.; Yang, X. Q.; Balasubramanian, M.; McBreen, J.; Xia, Y.; Sakai, T. *Journal of the Electrochemical Society* **2002,** 149, (7), A842-A848.
20. Berg, H.; Thomas, J. O. *Solid State Ionics* **1999,** 126, (3–4), 227-234.
21. Berg, H.; Rundlöv, H.; Thomas, J. O. *Solid State Ionics* **2001,** 144, (1–2), 65-69.
22. Gu, L.; Zhu, C.; Li, H.; Yu, Y.; Li, C.; Tsukimoto, S.; Maier, J.; Ikuhara, Y. *Journal of the American Chemical Society* **2011,** 133, (13), 4661-4663.
23. Huang, R.; Ikuhara, Y. H.; Mizoguchi, T.; Findlay, S. D.; Kuwabara, A.; Fisher, C. A. J.; Moriwake, H.; Oki, H.; Hirayama, T.; Ikuhara, Y. *Angewandte Chemie International Edition* **2011,** 50, (13), 3053-3057.
24. Lu, X.; Sun, Y.; Jian, Z.; He, X.; Gu, L.; Hu, Y.-S.; Li, H.; Wang, Z.; Chen, W.; Duan, X.; Chen, L.; Maier, J.; Tsukimoto, S.; Ikuhara, Y. *Nano Lett.* **2012,** 12, (12), 6192-6197.
25. Suo, L.; Han, W.; Lu, X.; Gu, L.; Hu, Y.-S.; Li, H.; Chen, D.; Chen, L.; Tsukimoto, S.; Ikuhara, Y. *Physical Chemistry Chemical Physics* **2012,** 14, (16), 5363-5367.
26. Sun, Y.; Zhao, L.; Pan, H.; Lu, X.; Gu, L.; Hu, Y.-S.; Li, H.; Armand, M.; Ikuhara, Y.; Chen, L.; Huang, X. *Nat Commun* **2013,** 4, 1870.
27. Winter, M.; Besenhard, J. O.; Spahr, M. E.; Novak, P. *Advanced Materials* **1998,** 10, (10), 725-763.
28. Zaghib, K.; Striebel, K.; Guerfi, A.; Shim, J.; Armand, M.; Gauthier, M. *Electrochimica Acta* **2004,** 50, (2-3), 263-270.
29. Shin, Y.; Manthiram, A. *Electrochimica Acta* **2003,** 48, (24), 3583-3592.
30. Tarascon, J. M.; Guyomard, D. *Journal of the Electrochemical Society* **1991,** 138, (10), 2864-2868.
31. Tarascon, J. M.; Guyomard, D. *Electrochimica Acta* **1993,** 38, (9), 1221-1231.
32. Brule, D. G.; Brown, J. R.; Bancroft, G. M.; Fyfe, W. S. *Chemical Geology* **1980,** 28, (3-4), 331-339.
33. Biesinger, M. C.; Payne, B. P.; Grosvenor, A. P.; Lau, L. W. M.; Gerson, A. R.; Smart, R. S. *Applied Surface Science* **2011,** 257, (7), 2717-2730.
34. Levi, M. D.; Gamolsky, K.; Aurbach, D.; Heider, U.; Oesten, R. *Journal of the Electrochemical Society* **2000,** 147, (1), 25-33.
35. Zhou, S. S.; Han, H. B.; Nie, J.; Armand, M.; Zhou, Z. B.; Huang, X. J. *Journal of the Electrochemical Society* **2012,** 159, (8), A1158-A1164.
36. Lin, F.; Markus, I. M.; Nordlund, D.; Weng, T. C.; Asta, M. D.; Xin, H. L. L.; Doeff, M. M. *Nature Communications* **2014,** 5.
37. Schmidt, J. P.; Chrobak, T.; Ender, M.; Illig, J.; Klotz, D.; Ivers-Tiffee, E. *Journal of Power Sources* **2011,** 196, (12), 5342-5348.
38. Wang, R.; He, X. Q.; He, L. H.; Wang, F. W.; Xiao, R. J.; Gu, L.; Li, H.; Chen, L. Q. *Advanced Energy Materials* **2013,** 3,

(10), 1358-1367.

39. Tang, D.; Sun, Y.; Yang, Z.; Ben, L.; Gu, L.; Huang, X. *Chemistry of Materials* **2014**. DOI: 10.1021/cm501125e

40. Kim, D.; Park, S.; Chae, O. B.; Ryu, J. H.; Kim, Y. U.; Yin, R. Z.; Oh, S. M. *Journal of the Electrochemical Society* **2012,** 159, (3), A193-A197.

41. Armstrong, A. R.; Dupre, N.; Paterson, A. J.; Grey, C. P.; Bruce, P. G. *Chemistry of Materials* **2004,** 16, (16), 3106-3118.

42. Mohanty, D.; Kalnaus, S.; Meisner, R. A.; Rhodes, K. J.; Li, J. L.; Payzant, E. A.; Wood, D. L.; Daniel, C. *Journal of Power Sources* **2013,** 229, 239-248.

43. Mohanty, D.; Sefat, A. S.; Li, J. L.; Meisner, R. A.; Rondinone, A. J.; Payzant, E. A.; Abraham, D. P.; Wood, D. L.; Daniel, C. *Physical Chemistry Chemical Physics* **2013,** 15, (44), 19496-19509.

44. Tarascon, J. M.; Guyomard, D. G.; Wilkens, B.; McKinnon, W. R.; Barboux, P. *Solid State Ionics* **1992,** 57, (1-2), 113-120.

45. Yabuuchi, N.; Yano, M.; Kuze, S.; Komaba, S. *Electrochimica Acta* **2012,** 82, 296-301.

46. Dai, Y.; Wang, K.; Xie, J. Y. *Applied Physics Letters* **2007,** 90, (10).

47. Mishra, S. K.; Ceder, G. *Physical Review B* **1999,** 59, (9), 6120-6130.

48. Reed, J.; Ceder, G. *Chemical Reviews* **2004,** 104, (10), 4513-4533.

49. Armstrong, A. R.; Paterson, A. J.; Dupre, N.; Grey, C. P.; Bruce, P. G. *Chemistry of Materials* **2007,** 19, (5), 1016-1023.

50. Raekelboom, E. A.; Hector, A. L.; Owen, J.; Vitins, G.; Weller, M. T. *Chemistry of Materials* **2001,** 13, (12), 4618-4623.

51. Robertson, A. D.; Bruce, P. G. *Chemical Communications* **2002**, (23), 2790-2791.

52. Robertson, A. D.; Bruce, P. G. *Chemistry of Materials* **2003,** 15, (10), 1984-1992.

53. Rana, J.; Stan, M.; Kloepsch, R.; Li, J.; Schumacher, G.; Welter, E.; Zizak, I.; Banhart, J.; Winter, M. *Advanced Energy Materials* **2014,** 4, (5).

Table of contents

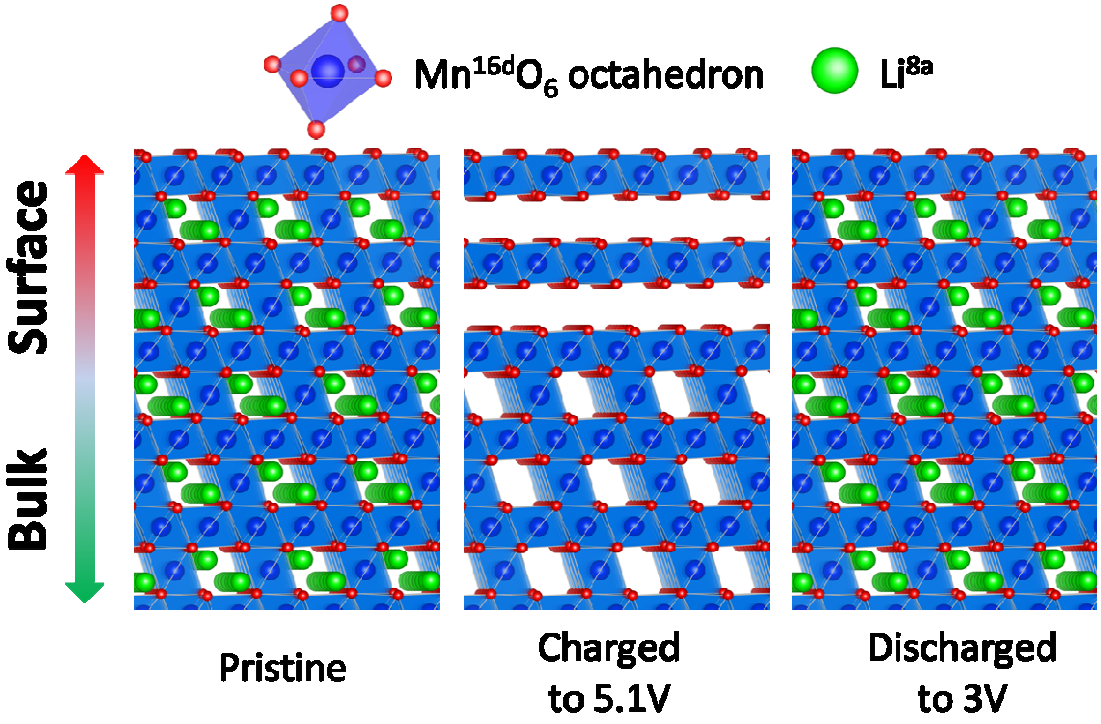

Charging spinel $LiMn_2O_4$ cathode material to high voltage (> 4.3 V) is a convenient way to obtain more lithium ions for formation of anodic solid-electrolyte-interface in a full cell. In this work, $LiMn_2O_4$ spinel cathode material was charged to 5.1 V for only one cycle during normal cycling (3-4.3 V) to study the impact of high voltage on the electrochemical performance and structure. The electrochemical performance showed that more lithium ions were de-intercalated from the cathode structure during cycling between 3-5.1 V. However, even cycled to high voltage for only one cycle, the surface of the cathode demonstrated a drastic change in atomic-level structure. Via an advanced scanning transmission electron microscopy (STEM), the formation of a layered-like phase was directly observed on the surface of spinel $LiMn_2O_4$ charged to high voltage, implying instability of the spinel structure at high charge voltage. This observation contradicts to the conventional wisdom that the spinel structure is more stable than the layered structure during lithium intercalation. X-ray photoelectron spectroscopy (XPS) results showed a small amount of manganese with lower oxidation states after being charged to 5.1 V, suggesting an accelerated speed of manganese dissolution.

Table of contents